Microfabricated water immersion zone plate optical tweezer

Ethan Schonbrun, Charles Rinzler, and Kenneth B. Crozier[a)]
School of Engineering and Applied Sciences, Harvard University, Cambridge, Massachusetts 02138, USA

(Received 5 December 2007; accepted 3 January 2008; published online 21 February 2008)

We demonstrate the trapping of beads in water with a microfabricated Fresnel zone plate. Beads are loaded onto the microfabricated optical traps using conventional optical tweezers and fluorescence microscopy is used to track bead position. Analysis of the bead position as a function of time is used to determine trapping stiffness. We present experiments showing the three-dimensional trapping of 2 μm diameter beads with trapping stiffnesses that are comparable to conventional optical tweezers when the zone plate efficiency is taken into account. © *2008 American Institute of Physics*. [DOI: 10.1063/1.2837538]

Optical tweezers use the forces exerted by tightly focused laser beams to trap and move objects with sizes ranging from tens of nanometers to tens of micrometers. Since the pioneering work of Ashkin *et al.* in 1986,[1] optical tweezers have become important tools in the biological sciences. Trapped particles can be used to exert forces on, or measure forces from, their local environments with calibration performed with Hooke's Law.[2] Well-calibrated traps have been used for quantitative observations of biological processes, including the motion of kinesin motor molecules[3] and the force generated by RNA polymerase as it moves along a DNA molecule.[4] Static arrays of optical traps have been employed for the continuous sorting of fluid-borne particles based on their differing affinities for the traps.[5] The incorporation of optical tweezers into microfluidic chips would provide new functionalities for these systems, such as particle sorting, particle manipulation, and biophysical force measurements. The short working distance (usually <200 μm), size, and cost of microscopic lenses used in conventional tweezers, however, make them impractical to integrate into microfluidic chips.

In this letter, we design and demonstrate the use of a Fresnel zone plate to produce well-calibrated optical traps in an integrated system. Because of their small size and ease of fabrication, future implementations could include large lenslet arrays[6] or embedding them deep inside microfluidic devices.[7] Fiber optical traps[8,9] and micromirror tweezers[10] are two other integrated geometries where large trapping forces have been measured. While both of these geometries do not require precision projection optics, the Hooke's spring constant was not measured and data was not presented for particles smaller than 6 and 9 μm, respectively. Recently, the use of surface plasmon field enhancements was demonstrated for integrated optical trapping,[11,12] but experiments have not yet been shown that exhibit tightly localized particles or stiff optical traps.

The zone plate is designed to be used at the glass/water interface of a sample cell. This allows the use of a short focal length design, enabling the numerical aperture to be close to its theoretical maximum, the refractive index of water. The diameter of the element is 100 μm and its focal length is 8 μm, yielding an effective numerical aperture (NA) of 1.31. The inner and outer radii of the concentric rings are given by $\sqrt{n\lambda f+n^2\lambda^2/4}$, where n is an integer, f is the focal length, and λ is the wavelength in water.[13] The starting substrate is a glass slide coated with a thin layer of indium tin oxide to prevent charging during lithography. Polymethylmethacrylate is spun on and exposed by e-beam lithography. Gold is evaporated to a thickness of 50 nm, with a thin layer of chrome used for adhesion. Lift-off is then performed, yield-

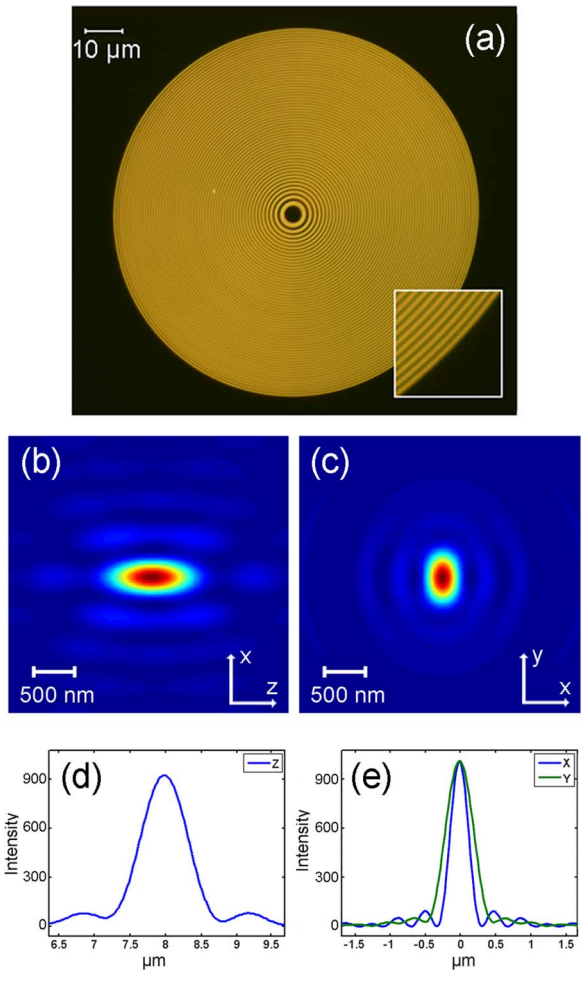

FIG. 1. (Color online) Fresnel zone plate fabrication and modeling. (a) Optical micrograph of fabricated zone plate. The bright regions are gold and the dark regions are glass. (b) Simulated axial (x-z plane) intensity distribution of the focal spot. (c) Cross section (x-y plane) of the transverse intensity at the focus 8 μm behind the zone plate. [(d) and (e)] Line section through the focus, where (d) plots as a function of the axial dimension and (e) plots as a function of the two transverse dimensions. The incident field is polarized in y which results in asymmetry of the focus. The peak intensity at the focus is 1000 times the peak intensity of the broad Gaussian illumination.

[a)]Electronic mail: kcrozier@seas.harvard.edu.

ing the device shown in the photograph of Fig. 1(a). The light regions are gold and the dark regions are glass areas where the gold has been removed.

The zone plate is designed for use with a free space illumination wavelength of $\lambda_0=976$ nm, corresponding to a wavelength in water of $\lambda=735$ nm. At the outermost ring, the period is 745 nm, which is slightly larger than λ. To model the performance, we use a two-dimensional split-step Fourier beam propagation (BP) algorithm.[14] A nonparaxial scalar code[15] is modified to account for the smaller than unity modulation depth of interfering vector field components. The zone plate is treated as a thin element and reflections from its surface are ignored. The propagation direction is taken as the z axis and the input beam is polarized along the y axis. Figure 1(b) shows a yz-plane cross section of the intensity through the beam focus, which yields an axial full width at half maximum (FWHM) of 764 nm along the z axis. Figure 1(c) shows a cross section of the intensity at the focal plane in the xy plane. The focal spot size has a FWHM of 302 nm along the x axis and 473 nm along the y axis. Around the focal region, there are numerous sidelobe peaks, but their peak intensity is less than 1/10 of the intensity of the central peak. The gold is modeled as a partially transmitting region with a transmission coefficient of 0.1.

While the zone plate only needs a collimated input laser beam to form a trap, additional optics are used in the experimental setup (Fig. 2) to load the trap effectively and to characterize its performance. Light from a fiber coupled diode laser ($\lambda_0=976$ nm) is collimated and focused onto the zone plate chip using a 200 mm focal length lens. This produces a spot with a diameter of 180 μm that overfills the 100 μm diameter of the zone plate. A liquid cell is formed by sandwiching a layer of water between the zone plate substrate and a coverslip. Fluorescent beads with diameters of 2 μm are trapped at the zone plate focus. A green laser ($\lambda_0=532$ nm) is used to excite fluorescent emission from the trapped beads, which are imaged by a microscope objective onto a charge coupled device (CCD) camera. As discussed further below, a trap based on a HeNe laser is used to load beads into the zone plate trap. A low-pass and a band-pass filter as well as dichroic mirrors are used to block the trapping, green, and HeNe lasers so that only the fluorescent emission is collected onto the CCD camera. A tungsten lamp is used for white light illumination.

The zone plate trap is loaded with a traditional optical tweezer that is incident from the opposite side of the sample chamber. Because the focal region is relatively close to the substrate surface, a tweezer that traps only transversely while pushing the particle against the substrate surface is adequate for loading. The loading trap consists of a HeNe laser (10 mW) focused by a microscope objective (0.8 NA). With this trap we can quickly load and measure the performance of the zone plate trap without having to wait for a particle to diffuse into the trap. Unlike traditional optical tweezers, once a particle is trapped by the zone plate, the sample cell can be translated tens of microns and the particle remains fixed with respect to the sample cell.

Once the zone plate trap is loaded, the green laser is turned on and the HeNe laser is turned off. Figure 3 shows a polystyrene bead (2 μm diameter) trapped by the zone plate. In this photograph, both the green laser and the lamp are on. The central rings of the zone plate are visible, although out of focus due to the fact that they are 8 μm behind the bead.

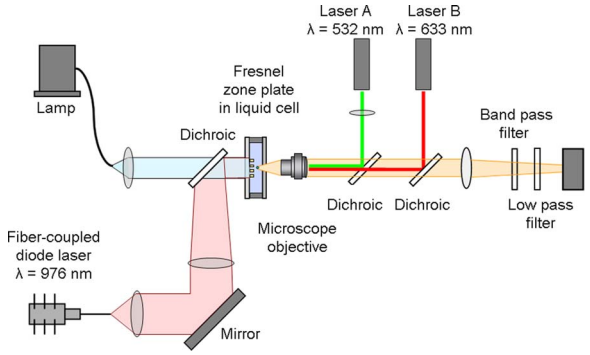

FIG. 2. (Color online) Schematic of Fresnel zone plate optical tweezer experimental setup.

After releasing a 2 μm diameter bead from the HeNe laser-based loading trap, we find that there is a ~50% probability that it will be trapped by the zone plate. In order to determine the trapping stiffness, movies of trapped beads are acquired at 30 Hz to capture the bead motion as a function of time. Centroid calculations are performed on the images to monitor the bead position.

For an object in a harmonic potential with stiffness k_{trap}, the equipartition theorem states that[2]

$$\frac{1}{2}k_B T = \frac{1}{2}k_{\text{trap}}\langle (x - x_{\text{mean}})^2 \rangle, \tag{1}$$

where k_B is Boltzmann's constant, T is absolute temperature, and $\langle (x-x_{\text{mean}})^2 \rangle$ is the variance of the particle from its trapped equilibrium position. Knowledge of the particle's instantaneous position as a function of time therefore enables the stiffness k_{trap} to be determined. However, detection systems such as CCD cameras and photodiodes do not measure the instantaneous position of a particle. The measured position is an average of the true position over the integration time, leading to motion blur. This introduces a systematic bias into the measured variance, although it has been recently shown that this can be corrected.[16] The true and measured variances var(X) and var(X_{expt}) are related by[16]

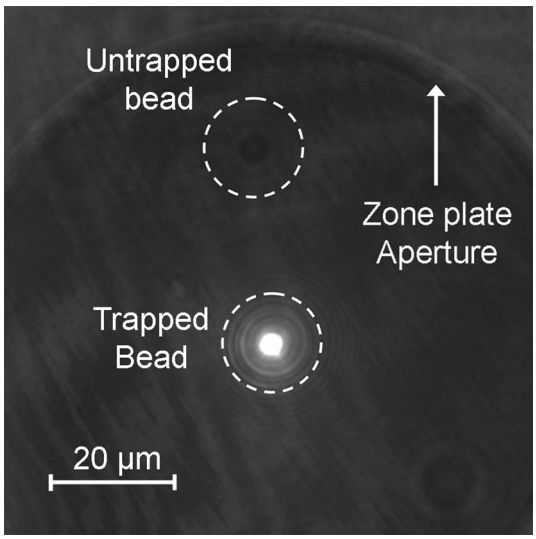

FIG. 3. Photographs of 2 μm diameter beads trapped by zone plate. White light illumination and a green laser (for fluorescence excitation) are used. Bead is trapped 8 μm above the zone plate surface, which appear slightly out of focus.

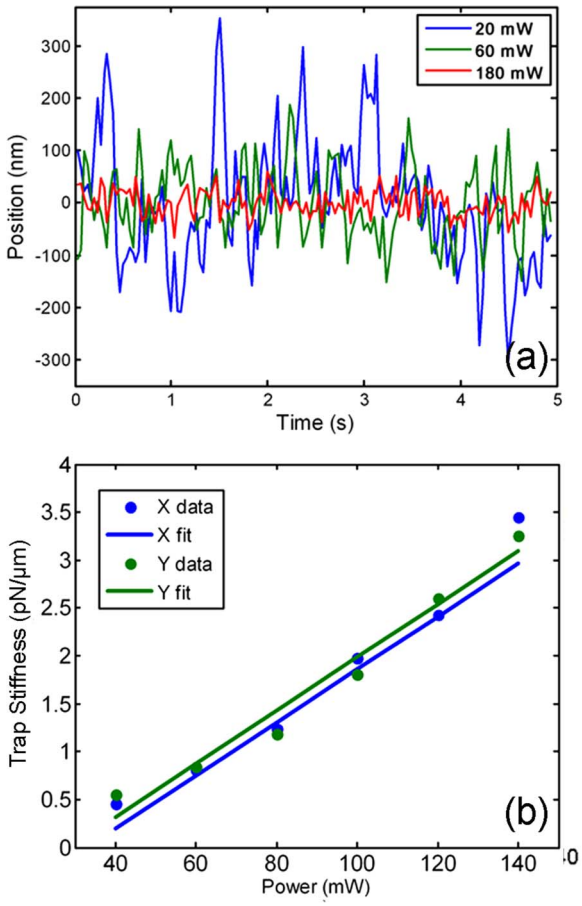

FIG. 4. (Color online) Zone plate performance: experimental data. (a) Bead position along x axis as a function of time for different laser powers. (b) Trap stiffness k_{trap} along x and y axes as a function of laser power. The stiffnesses of 0.0294 pN/μm mW and 0.0277 N/μm mW along the x and y axes, respectively, are found by linear fits to the data using a least squared regression.

$$\mathrm{var}(X_{\mathrm{expt}}) = \mathrm{var}(X) S(k_{\mathrm{trap}}, W, \tau), \tag{2}$$

where $S(k_{\mathrm{trap}}, W, \tau)$ corrects for motion blur. It is a function of k_{trap}, the exposure time W and the relaxation time τ. The exposure time W used in the experiments is 1/64 s. The relaxation time is given by $\tau = 2\pi\gamma/k_{\mathrm{trap}}$, where γ is the Stoke's drag coefficient. To determine k_{trap}, we combine Eqs. (1) and (2) to give

$$\mathrm{var}(X_{\mathrm{expt}}) = \frac{k_B T}{k_{\mathrm{trap}}} S(k_{\mathrm{trap}}, W, \tau). \tag{3}$$

This equation is solved numerically to find k_{trap} from the measured variance $\mathrm{var}(X_{\mathrm{expt}})$.

Figure 4(a) shows three traces of the bead position for laser powers of 20, 60, and 180 mW. As expected, the variance of the bead position is inversely proportional to laser power. The measured trap stiffness, with motion blur corrected for, is plotted in Fig. 4(b) as a function of laser power, which ranges from 40 to 140 mW. A linear fit of the curves shows that the power-normalized stiffness is 0.0294 pN/μm mW along the x axis and 0.0277 pN/μm mW along the y axis. There is an offset in the linear fit that results in a zero trap stiffness at 31 and 28 mW for the x and y curves, respectively. At powers below these values, we found that stable trapping occurred, but cannot be described by the linear fit because the trap is no longer harmonic at this shallow depth. At the highest laser powers, the stiffness also deviates from linear. At powers of 160 and 180 mW, the trapping stiffness continued to increase, but convection currents in the trap tend to destabilize the performance.

Overfilling the zone plate aperture reduces the trap intensity by a factor of 4, which then gives the zone plate trap a stiffness of approximately one tenth of the theoretical optimum of 1 pN/μm mW (Ref. 17) for a 2 μm polystyrene sphere using a 1.4 NA objective lens. This factor of 10 can be traced to the diffraction efficiency of a binary amplitude grating, which is $1/\pi^2$.[14] By using a π phase zone plate, the stiffness could be increased by an additional factor of 4. Even at the zone plate's current stiffness value, it compares well to high performance traps which frequently have values of 0.16 pN/μm mW.[2]

The focusing optic is the single most important element in an optical trap,[2] and in this report we have presented a substantial modification to the traditional experiment. Considerable flexibility can be added to optical tweezer experiments by taking advantage of a zone plate's much smaller cross section, thickness, and weight. Optical traps can be embedded deep inside fluidic chambers without the limitation of an immersion objective's small working distance. In addition, the fact that the trapping is decoupled from imaging allows traps to be translated, while remaining fixed relative to the substrate. We have experimentally shown that zone plate optical tweezers have comparable stiffness to traditional optical tweezers and, because of the flexibility of the lithographic process, this element can be further designed to implement functions that objective lenses cannot.

This work was supported by the Microsystems Technology Office (MTO) of the Defense Advanced Research Projects Agency (DARPA) and the Harvard Nanoscale Science and Engineering Center (NSEC) of the National Science Foundation (NSF). The authors thank Emre Togan for discussions on fabrication and Matthew Lang and David Appleyard for discussions on optical tweezers.

[1] A. Ashkin, J. M. Dziedzic, J. E. Bjorkholm, and S. Chu, Opt. Lett. **11**, 288 (1986).
[2] K. C. Neuman and S. M. Block, Rev. Sci. Instrum. **75**, 2787 (2004).
[3] S. M. Block, L. S. B. Goldstein, and B. J. Schnapp, Nature (London) **348**, 348 (1990).
[4] H. Yim, M. D. Wang, K. Svoboda, R. Landick, S. M. Block, and J. Gelles, Science **270**, 165 (1995).
[5] P. T. Korda, M. B. Taylor, and D. G. Grier, Phys. Rev. Lett. **89**, 128301 (2002).
[6] D. Gil, R. Menon, and H. I. Smith, J. Vac. Sci. Technol. B **21**, 2956 (2003).
[7] D. Psaltis, S. R. Quake, and C. Yang, Nature (London) **442**, 381 (2006).
[8] A. Constable, J. Kim, J. Mervis, F. Zarinetchi, and M. Prentiss, Opt. Lett. **18**, 1867 (1993).
[9] S. D. Collins, R. J. Baskin, and D. G. Howitt, Appl. Opt. **38**, 6068 (1999).
[10] F. Merenda, J. Rohner, J.-M. Fournier, and R.-P. Salathe, Opt. Express **15**, 6075 (2007).
[11] G. Volpe, R. Quidant, G. Badenes, and D. Petrov, Phys. Rev. Lett. **96**, 238101 (2006).
[12] M. Righini, A. S. Zelenina, C. Girard, and R. Quidant, Nat. Phys. **3**, 477 (2007).
[13] E. Hecht, *Optics*, 2nd ed. (Addison-Wesley, Reading, Massachusetts, 1987).
[14] J. W. Goodman, *Introduction to Fourier Optics* (McGraw-Hill, New York, 1996).
[15] J. E. Harvey, Am. J. Phys. **41**, 974 (1979).
[16] W. P. Wong and K. Halvorsen, Opt. Express **14**, 12517 (2006).
[17] N. B. Viana, A. Mazolli, P. A. Maia Neto, H. M. Nussenzveig, M. S. Rocha, and O. N. Mesquita, Appl. Phys. Lett. **88**, 131110 (2006).